Journal of Ovonic Research Vol. 14, No. 5, September – October 2018, p. 371 - 379

# THERMAL PROPERTIES OF PARAFFIN/ NANO-MAGNETITE-TREVORITE PHASE CHANGE MATERIALS

F. R. SAEED, M. H. A. A. AL-TIMIMI, W. H. A. AL-BANDA,
M. Z. ABDULLAH, I. STAMATIN, S. VOINEA, B. DOBRICA, A. E. BALAN*
*University of Bucharest, Faculty of Physics, 3Nano-SAE Research Centre, 405 Atomistilor str., PO Box MG-38, Bucharest-Măgurele, Romania*

Storage of latent heat using organic phase change nano-composite materials based on paraffin-nanoparticles shows a growing interest in thermal energy storage systems. Paraffin low thermal conductivity is the main drawback associated with such applications. To tackle this issue, a composite material based on paraffin with magnetite-trevorite nanoparticles dispersed in different ratios (0.5-2%) in paraffin has been studied. The nanoparticles were synthesized using co-precipitation method with microwave heat treatment and their structure and morphology were investigated by X-ray diffraction and scanning electron microscopy. Differential scanning calorimetry was used to identify the thermal properties of the composite materials. A special test rig was designed to investigate the effect of nanoparticles addition on the heat transfer rate as well as melting front velocity and charging time. Results show an acceptable thermal behavior of the composite, which makes it a candidate for heat transfer improvement in thermal energy storage applications.

(Received June 18, 2018; Accepted October 4, 2018)

*Keywords:* Phase change material, Nanoparticles, Thermal energy storage

## 1. Introduction

Phase change materials (PCMs) attracted considerable attention as a part of thermal energy storage applications. PCMs have the ability to absorb and release thermal energy during phase changing at almost constant temperature. Storage of energy through latent heat is the main motive behind applying of PCMs such as paraffin in many applications like solar energy, building energy saving, and thermal management systems of electronic devices. However, low thermal conductivity associated with using of organic PCMs can consider a vital obstacle in the way of using organic PCMs. Fins [1-2], metal foam [3], and fine particles are the most used techniques for thermal conductivity enhancement.

Particularly, nanoparticle addition has drawn attention to researchers over the last years. A nano-copper particle dispersed in water inside a square storage model was presented as one of the first numerical reports on nano-fluid solidification [4]. The evolution of solid/liquid interface was detected for pure PCM and for PCM/nano-copper, showing no effective increase in speed of the melting front phase interface at earlier stages of solidification due to nanoparticles addition. However, the impact of nano-copper particles was more effective at the melting interface with higher mass fractions. Numerical results showed that the melting rate of paraffin was enhanced after adding nanoparticles, i.e. adding 1 wt% Cu nanoparticles saves 13.1% of the melting time of paraffin, in agreement with previous researches [5].

An experimental and numerical study on melting of n-octadecane/CuO nanoparticles was performed in a square enclosure supplied to constant heat flux from one side and thermally insulated from the other sides [6]. Finite element method (FEM) was used to solve the coupled continuity, momentum, and energy equations in the numerical part. Both of experimental and numerical results evidence an improvement in thermal conductivity as a result of CuO nanoparticles effect, which leads to an increase of the heat transfer rate, in other words minimizing

*Corresponding author: andronie@3nanosae.org

the charging time. Also, they have discussed the agglomeration and precipitation impact at high loadings of nanoparticles due to viscosity increase.

Mesoporous silica dispersed in n-octadecane as PCM for thermal energy storage (TES) applications was achieved [7]. Results indicate that the thermal conductivity has been improved, for both liquid/solid phase in range of temperatures between 5-55 ˚C. On the other side, the viscosity increased with 60% relative to simple PCM for 5wt% loading at 35 ˚C.

Carbon nanomaterials were also used to enhance the thermal conductivity of phase change material, such as single walled carbon nanotube (SWCNT) [8], multi walled carbon nanotube (MWCNT) [9] and graphene [10]. Results showed that specific heat increased with increasing specific surface area of nano-materials, which can enhance the specific heat with 18.57% of carbonate salt (CPCM). Thermal conductivity of CPCM promoted to the 56.98% with addition of columnar structure of nano-materials such as SWCNT. All nanoparticle additives have limited effect on the total amount of thermal TES capacity [11]. Nanoparticle constriction (i.e. the contact area between linked nanoparticles) was also studied. Effective thermal conductivity of different MWCNT/ paraffin nano-composites was measured. The rate of heat transfer between the contacting MWCNTs can be increased by the factor 27, with diameter around 58nm [12].

The effect of nano-magnetite ($Fe_3O_4$) on thermal behavior of paraffin wax as PCM has been studied. Synthesis of nano-magnetite had been achieved by sol-gel method. They indicate an improvement in thermal conductivity by 48% and 67% for 10% and 20%, respectively. A slight improvement in latent heat capacity was also recorded, while melting temperature of the mixture was stable [13]. Moreover, another study on $Fe_3O_4$ nanoparticle enhanced paraffin wax showed that nanoparticle addition induces modifications in the activation energy of the melting process [14].

In the present work, authors propose a new composite: paraffin with magnetite-trevorite obtained by a simplified co-precipitation method, combined with microwave heat treatment. Nano-particles structure affected directly by thermal treatment during the synthesis. Microwave heat treatment can play essential role on the shape [15], size [16], and evolution of the synthesis process [17]. The aim of this work is investigate the effect of magnetite-trevorite particles on thermal behavior of paraffin. Different nanoparticle loadings were added into paraffin wax by mixing and melting processes. Thermal properties of the composites were measured experimentally in terms of latent heat and heat capacity and heat transfer rate.

## 2. Experimental

### 2.1 Materials

Materials used in this research work were paraffin (RT58, Sigma Aldrich), ferrous chloride ($FeCl_2.4H_2O$ Merck, 98%), nickel chloride ($NiCl_2.6H_2O$, Merck, 99.9%), ethylene glycol, Merck, 99.8%), sodium hydroxide (NaOH, pellets for analysis, Merck), hydrazine ($N_2H_4.H_2O$, Merck, 64-65 %, reagent grade, 98%), de-ionized distilled water was used in the preparation of all the solutions.

### 2.2 Synthesis of magnetite / trevorite compound

Nanoparticles synthesis was achieved by co-precipitation method based on chemical reduction of metals chlorides. 3.2g of $FeCl_2.4H_2O$ and 0.8g of $NiCl_2.6H_2O$ at molar ratio Fe/Ni 5/1 were dissolved in 100 ml of ethylene glycol of (99%). Afterwards, a mixer of high ultra-sonic frequency was used to disperse the metals chlorides in ethylene glycol. The reducing agent- 2M NaOH solution- is added dropwise to set the pH between 10 and 10.5 during stirring at 6000rpm. The resulting solution is then subjected to microwave heat treatment at 140 ˚C for 40 minutes. The pH of the solution is adjusted to 10.5-11 by adding hydrazine. Finally, microwave heat treatment was applied again to the solution for 2 hours at 100 ˚C that results in black powder precipitation of magnetite/trevorite nanoparticles. The precipitate particles are washed with distillated water repeatedly until pH 7 and dried in an air oven for 24 hour at 50 ˚C.

### 2.3 Preparation of Paraffin / Nano M-T nanoparticles mixture

Paraffin / magnetite-trevorite composite was prepared by dispersion and melting procedures. Paraffin is melted at 70$^{o}$C for 50 minutes and, then, magnetite/trevorite particles are mixed into the paraffin using an ultrasonic bath for 2 hours. Three different loadings of nanoparticles: 0.5, 1, and 2 wt% are added to the liquid paraffin to form the composite.

### 2.4 Characterization methods

The synthesized nanoparticles were characterized by XRD analysis of Panalytical X'pert PRO MPD equipment, with the following operation conditions, the 2theta interval: 35-120 deg, step size 0.02 grade, time/step = 2 sec, 40 mA current and 45 kV voltage. The morphology and microstructure of the nanoparticles are characterized using Scanning Electron Microscopy (SEM, JIB-4600F), with 20 kV of tension acceleration. Thermal analysis are performed by means of differential scanning calorimeter (DSC Mettler Toledo, model Star1) in nitrogen atmosphere at 10$^{o}$C/min heating rate, in the temperature range 20-90$^{o}$C. The 5-10 mg samples are sealed in aluminium pans. Indium was used as a calibration reference of DSC. Each sample was treated for 30 min at 90$^{o}$C to lose the thermal memory effect. The heat transfer rate during melting and the effect of nanoparticles adding to the paraffin on thermal conductivity properties were investigated through an in-house test rig. The schematic representation of experimental setup of rectangular container is shown in Fig. 1. The test rig enclosure is made of fiberglass plates with internal dimensions of 100 × 25 × 20 mm. The thermal conductivity of the fiberglass is about 0. 4 W/m.K, which can consider its low enough to reduce heat losses from the test rig.

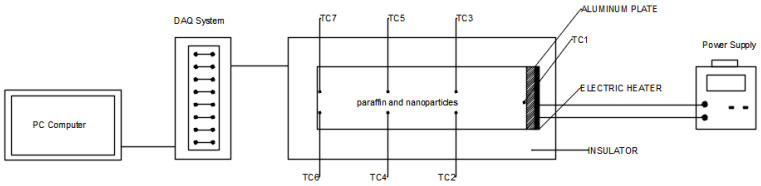


*Fig. 1. Schematic diagram for the experimental setup.*

*Table 1. (x, y) coordinates of the thermocouples in mm for the test rig.*

| | | | |
|---|---|---|---|
| ***TC1*** *(1,9)* | ***TC3*** *(33,18)* | ***TC5*** *(66,18)* | ***TC7*** *(99,18)* |
| | ***TC2*** *(33,8)* | ***TC4*** *(66,8)* | ***TC6*** *(99,8)* |

An aluminum plate of high thermal conductivity (218 W/m.K) is fixed on the right side of the rectangular enclosure to obtain uniform heat flux applied on the plate by an electric heater. The 0.254 mm- thick electric heater has a maximum heat flux of about 1.55x10$^{4}$ W/m$^{2}$ at 120 V. This heater is firmly attached to the outer surface of the aluminum plate. A power supply is applied to perform the constant heat rate as the voltage can be changed while the electric current changes. Seven K-type thermocouples (TCs) with 0.26 mm bare wire diameter were used for monitoring the temperature of the sample inside the container. TCs were positioned at different locations by using clear epoxy (see Table 1). 8-channel data acquisition (PICO) unit was used to record the TCs readings. The Data Logger unit was connected to a computer and operated through a data recorder program. Prior measurements, TCs were calibrated.

## 3. Results and discussions

### 3.1 XRD

Debye-Scherrer formula was used to calculate the average crystalline size of the synthesized nano-particles which was around 10 nm. The identification of the peaks was carried out using data base ICCD (International Center for Diffraction date) with the pdf card for the nickel-Iron-oxide 04-014-8285. Calculating the size of crystallization by considering Nickel-Iron

oxide diffraction peaks (2θ = 35.68˚), corresponding to Miller indices (311). This is revealed that the resultant particles were face-centered cubic (fcc), on the other hand the second identification was achieved with the pdf card for $Fe_3O_4$ (magnetite) 04-016-4197. The crystallize size of the second material was obtained by considering Iron oxide $Fe_3O_4$ diffraction peak (2θ= 34.75˚), corresponding to Miller indices (230). This is revealed that the resultant particles were orthorhombic [18].

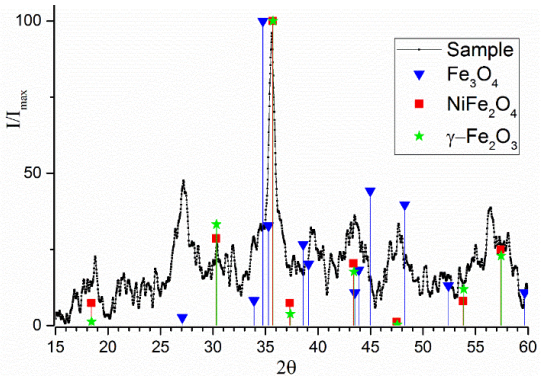


*Fig. 2. XRD diffractogram of nano-magnetite-trevorite.*

### 3.2 Morphology, topography, structure and phases

At a first glance SEM images recorded on the synthesis products show particles with irregular shapes (see Fig. 3). A detailed analysis at downscale reveals spongy-like structures consisting of nanoparticles form the spongy structure. Table 1 shows the composition analysis of the nano-magnetite-trevorite compound powder obtained by EDX test. The EDX results confirm the percentage ratio of Fe, Ni, and O, in the synthesized composite.

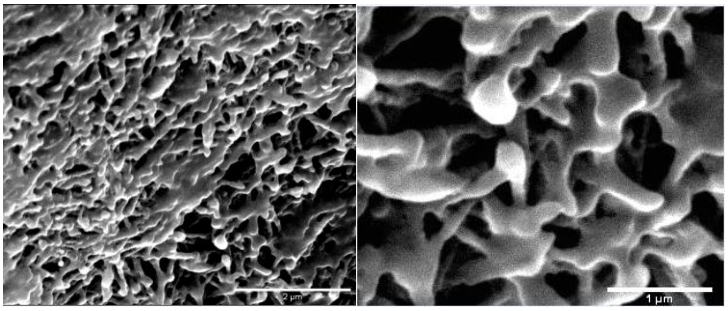


*Fig. 3. SEM image of magnetite-trevorite nanoparticles.*

*Table 2. EDX analysis of magnetite-trevorite nanoparticles.*

| ***Element*** | ***Weight (%)*** | ***Atomic (%)*** | ***Error (%)*** |
|---|---|---|---|
| *O K* | *11.91* | *32.15* | *6.35* |
| *Fe K* | *81.13* | *62.73* | *1.68* |
| *Ni K* | *6.96* | *5.12* | *3.71* |

### 3.3 Thermal analysis

Thermal analysis of pure paraffin and paraffin/ nano-magnetite-trevorite compound was tested at various loadings of nano-magnetite-trevorite particles 0wt%, 0.5wt%, 1wt%, and 2wt% with 10$^{o}$C/min heating and cooling rate (see Fig. 4). The phase transition for both, solid-solid phase occurring at lower temperature and solid-liquid phase at higher temperature were distinguished. The magnetite/trevorite particles impact on solidification and melting temperatures

of the composite are exposed in Table 3. The table readings show a slight change in the results of solidification and melting temperatures under the effect of nano-magnetite-trevorite particles. Solid-solid transition occur at 35.46°C, followed by solid–liquid transition at 52.34°C. $T_t$ is the phase change temperatures measured during heating and cooling were denoted as the transition temperature, $T_m$ is the melting temperature and $T_c$ is the crystallization temperature, respectively. The first peak appear at solid-solid transition can be interpreted a monoclinic crystal disordering to a pseudo-hexagonal crystal before isotropization of the melt which is a paraffin property [19].

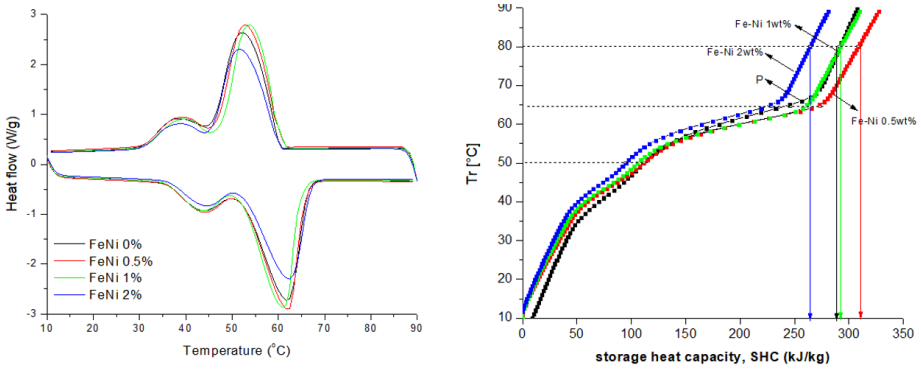


*Fig. 4. (left) DSC thermograms of paraffin with different loadings of magnetite/trevorite particles (^exo); (right) SHC heat storage in paraffin- magnetite/trevorite particles composites for different wt.% loadings. (FeNi-0, FeNi -0.5, FeNi -1, and FeNi -2,) with the heating and cooling rate of 10°C/min.*

Table 3 indicates the enthalpy of pure paraffin and various ratios of paraffin/nano-magnetite-trevorite composite. The enthalpy of the samples was estimated by integrating the area under the DSC curve. Fig. 4 (left) indicates the storage heat capacity (SHC) of pure paraffin and paraffin/nano-magnetite-trevorite particles. Results shows that SHC increased for lower concentration and decreased for higher nanoparticle loadings. Latent heat is a crucial factor for PCMs, since it determines the thermal capacity. Latent heat improvement detected at 0.5wt% loading of nano-magnetite-trevorite particles can be attributed to the high surface area of the nanoparticle which leads to an intermolecular interaction with the surrounding medium. Another factor improving the surface interaction paraffin/ nano-magnetite-trevorite compound is the different coordination geometry of nano-magnetite-trevorite particles structure related to surface defect sites [20]. Previous researches have evidenced also enhancement of latent heat when adding different nano-materials, such as carbon nanotubes and nano-$SiO_2$ to PCM [21-22].

*Table 3. The transition temperature $T_t$, melting temperature $T_m$, crystallization temperature $T_c$ and latent heat of the pure paraffin and the mixtures*

| **Sample** | **%wt FeNi** | **$T_t$ (°C)** | **$T_m$ (°C)** | **$T_c$ (°C)** | **ΔH (J/g)** |
|---|---|---|---|---|---|
| FeNi-0% | 0.00 | 35.46 | 52.34 | 60.46 | 112.99 |
| FeNi -0.5% | 0.50 | 35.90 | 52.29 | 60.79 | 116.22 |
| FeNi -1% | 1.00 | 35.68 | 52.35 | 60.59 | 112.51 |
| FeNi -2% | 2.00 | 36.14 | 52.40 | 60.35 | 98.44 |

*Table 4. Specific heat capacities of the solid and liquid phase at (s, 15 °C) and (l, 80 °C).*

| **Sample** | **FeNi -0%** | **FeNi-0.5%** | **FeNi -1%** | **FeNi -2%** |
|---|---|---|---|---|
| Cp (s, 15 °C)(J/g.K) | 1.569 | 1.669 | 1.555 | 1.434 |
| Cp (l, 80 °C) (J/g.K) | 1.932 | 2.047 | 1.933 | 1.797 |

The activation energy of the phase transitions is estimated by Kissinger method, using DSC data of heating the paraffin based samples at different heating rates and plotting *ln* $(V/T_p^2)$ as function of $1000/T_p$ [23] (Fig. 5), where $V$ is the heating rate ($^oC/s$) and $T_p$ the peak temperature (K). The activation energy ($E_a$) is calculated from the slope of the linear fit of the graph and is defined as the least required energy for attaining the specific phase transition.

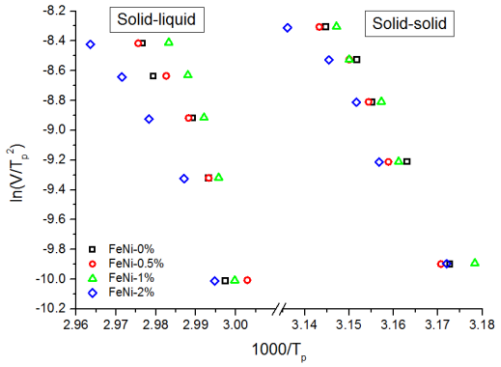


*Fig. 5. Graph ln (V/Tp2) vs. 1000/Tp. - Kissinger method for the paraffin- magnetite-trevorite mixtures.*

Table 5 expose the activation energy, pre-exponential factor and correlation coefficient. The results shows a slight change of activation energy for both solid-solid and solid-liquid phase transitions with various nanoparticles loadings. One can note an increase of the activation energy value for the solid-liquid transitions in 0.5-1 wt.% nanoparticle loading. This increasing tendency is correlated with thermal analysis results that the composite material has a higher latent heat. The nano-magnetite-trevorite dispersed into the organic lamellar phase may change the dynamics of the melting process since the nanoparticles acted as a thermal hinder in the paraffin matrix.

*Table 4. The activation energy, pre-exponential factor, and correlation coefficient.*

| | | Solid-Solid | | | Solid-Liquid | | |
|---|---|---|---|---|---|---|---|
| **Sample** | **%wt. FeNi** | **$E_a$ (kJ/mol)** | **ln A** | **R** | **$E_a$ (kJ/mol)** | **ln A** | **R** |
| FeNi -0% | 0.0 | 480±36 | 184.46 | 0.98 | 398±72 | 145.10 | 0.91 |
| FeNi -0.5% | 0.5 | 504±38 | 193.49 | 0.98 | 495±48 | 180.11 | 0.96 |
| FeNi -1% | 1.0 | 421±33 | 161.84 | 0.97 | 594±83 | 284.16 | 0.94 |
| FeNi -2% | 2.0 | 384±35 | 147.48 | 0.97 | 413±53 | 149.83 | 0.94 |

### 3.4 Heat transfer rates

Heat transfer rates for the nano-magnetite-trevorite-enhanced paraffin have been investigated using the experimental test rig that provides constant heat flux from one side of the enclosure while the rest is thermally insulated. The required time to achieve melting is recorded for various loadings of particles by studying the evolution of the temperature values at different locations inside the cell (Fig. 6). The recorded results present a decrease in the charging time with increasing loadings compared to pure paraffin: 28.0%, 30%, and 34% for the 0.5wt.%, 1wt.%, and 2wt.% loadings respectively (Table 5). However, results show an increase in heat transfer rates in the range 0.5 to 1wt.%, while in the range 1 to 2wt.% the transfer rates show a slight increase. This can be explained as a decrease in the impact of natural convection in the melt fraction due to an increase in dynamic viscosity, or as agglomeration and precipitation occurring at high

nanoparticles loadings. In some cases, the effects of high viscosity may exceed the enhancement in heat transfer rates, as observed both experimentally and numerically in past research [24-25].

*Table 5. Time duration of a single melt cycle, as recorded by TC6.*

| Sample | FeNi Loading [wt.%] | Melting point $T_m$ [°C] | Time until melting [s] |
|---|---|---|---|
| FeNi -0% | 0.0 | 55.00 | 9183 |
| FeNi -0.5% | 0.5 | 55.01 | 6595 |
| FeNi -1% | 1.0 | 55.01 | 6426 |
| FeNi -2% | 2.0 | 55.02 | 6023 |

Readings obtained by the attached thermocouples show that the temperatures in the upper part of the test cell (TC3, TC5, and TC7) are generally higher than the lower part due to the strong natural convection currents, which begin within the melted paraffin next to the active heated wall. The direction of the convection currents is clockwise in the direction of the solid-liquid interface. When these currents reach the interface, thermal energy is transferred from the liquid phase toward the solid phase, and the resident liquid phase becomes colder. The density of the cold phase is lower than the hot phase, which forces the liquid to descend along the interface from the upper part toward the lower part of the test rig, as recorded by TC2, TC4, and TC6 (high temperature difference between the temperature readings on the upper and lower part of the test rig). On the lower part of the cell, diffusive heat transfer is dominant, while on the upper part convective heat transfer takes over. The velocity of the melting front phase increases with raising the loading of the nano-magnetite-trevorite particles (Figure 6), which lead in minimizing the charging time of the composite. One can note an improvement in the meting front phase velocity with addition of the nanoparticles and the maximum reading recorded at 2wt% of the nanoparticles ratio.

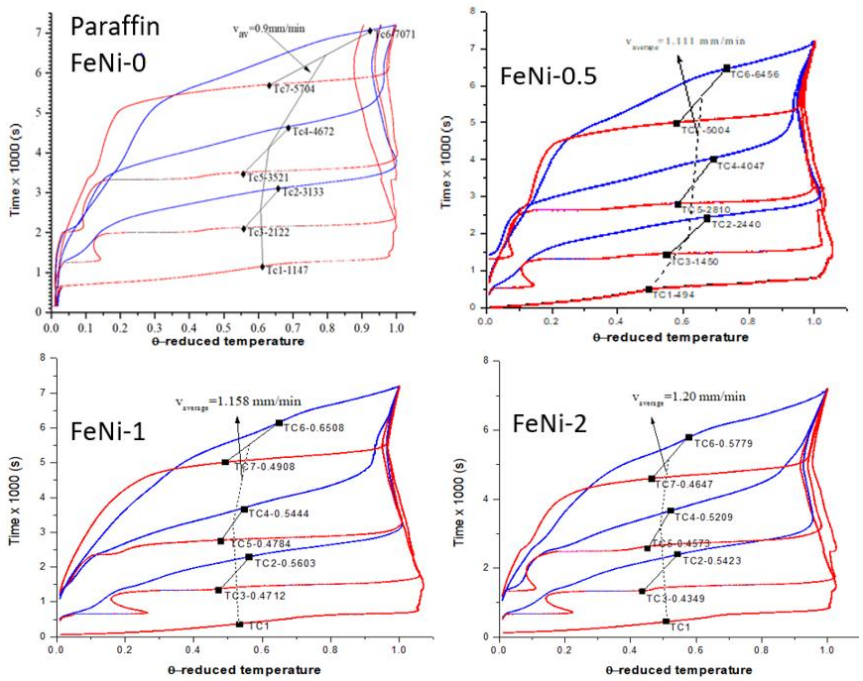


*Fig. 6. Paraffin, FeNi-0.5wt, 1wt%, and 2 wt.%: Temperature evolution for the seven thermocouples inside the test rig and the velocity of the melting front phase of paraffin II with different values of the Fe-Ni particles additives.*

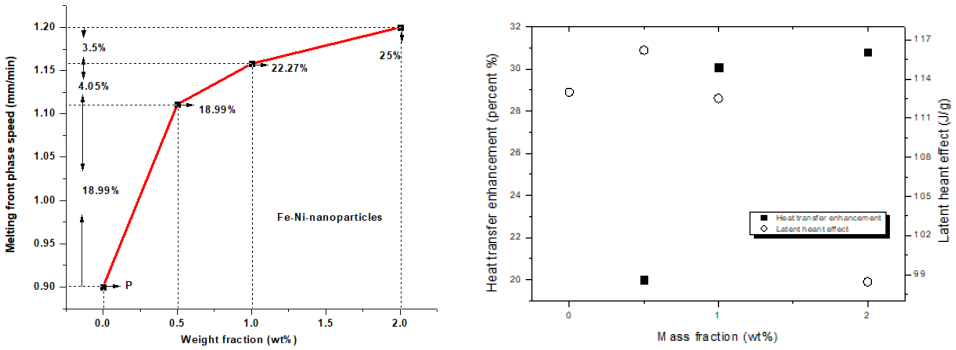


*Fig. 7. Latent heat and thermal conductivity of the paraffin/FeNi as a function of mass fraction (left); velocity of the melting front phase with different nanoparticles loadings(right).*

## 4. Conclusions

In summary, we have demonstrated that magnetite-trevorite composite with low loadings have an effective role in thermal energy storage applications. Slight enhancement in latent heat was detected with specific loading of nanoparticles 0.5wt%, while higher loadings did not determine an increase compared to pure paraffin. The same behavior was found in SHC. Improvement in latent heat and SHC can be explained by the high surface area to the volume, and by the surface defect sites of nano-magnetite-trevorite compound introduced by different geometry conditions. The fact of keeping the latent heat and specific heat capacity at the same level after the nanoparticles addition make it suitable to be tested for heat transfer improvement of paraffin. Results of the effect of nanomagnetite-trevorite addition on the thermal properties prove an increase in the melting front phase velocity due to the charging time decrease with increasing the nanoparticle content. However the percent of improvement of the melting front phase velocity was reduced with the higher concentration which can be interpreted as a result for agglomeration or increasing the viscosity of the used mixture.

### Acknowledgements

This work was supported by the Ministry of Science and Technology in Baghdad and by the Romanian Space Agency, Star Program, project no. 134/2017.

## References

[1] Z. Liu, X. Sun, C. Ma, Energy Conversion and Management **46**, 959 (2005).
[2] V. Shatikian, G. Ziskind, R. Letan (2008), International Journal of Heat and Mass Transfer **51**, 1488 (2008).
[3] X. Tong, Jamil A. Khan, M. RuhulAmin, International Journal of Computation and Methodology **30** (2), 125 (1996).
[4] J. M. Khodadadi, S. F. Hosseinizadeh, International Communications in Heat and Mass Transfer **34**, 534 (2007).
[5] S. Wu, H. Wang, S. Xiao, D. Zhu, Procedia Engineering **31**, 240 (2012).
[6] S. Nabeel, J. Khodadadi, A. Tahseen, International Journal of Heat and Mass Transfer **66**, 672 (2013).
[7] S. Motahar, N. Nikkam, A. A. Alemrajabi, R. Khodabandeh, M. S. Toprak, M. Muhammed, International Communications in Heat and Mass Transfer **56**, 114 (2014).
[8] S. Shaikh, K. Lafdi, K. Hallinan, Journal of Applied Physics **103**, 094302 (2008).
[9] J. Wang, H. Xie, Z. Xin, Thermochimica Acta **488**, 39 (2009).
[10] F. Yavari, F. H. Raeisi, K. Pashayi, M. A. Rafiee, Zamiri, Z. Yu, et al., Journal of Physical

Chemistry C **115**, 875 (2011).
[11] Y. Tao, C. Lin, Y. He, Energy Conversion and Management **97**, 103 (2015).
[12] J. Ronald, S. Amy, Applied Energy **154**, 271 (2015).
[13] Ş. Nurten, F. Magali, P. Halime, Solar Energy Materials & Solar Cells **137**, 61 (2015).
[14] F. R. Saeed, E. C. Serban, E. Vasile, M. H. A. A. Al-Timimi, W. H. A. Al-Banda, M. Z. A. Abdullah, I. Stamatin, A. Cucu, S. M. Iordache, S. Voinea, A. E. Balan, Digest Journal of Nanomaterials and Biostructures **12**(2), 273 (2017).
[15] T. Krishnakumar, N. Pinna, K. Prasanna Kumari, K. Perumal, R. Jayaprakash, Materials Letters **62**, 3437 (2008).
[16] L. Zhang, K. Lee, J. Zhang, Electrochimica Acta **52**, 3088 (2007).
[17] Z. Karcioglo, R. Boncukcuoglu, I. H. Karakaab, M. Ertugrul, Journal of Magnetism and Magnetic Materials **374**, 298 (2015).
[18] S.-H. Wu, D.-H. Chen, Journal of Colloid and Interface Science, **259**, 282 (2003).
[19] S. Y. Chazhengina, E. N. Kotelnikova, I. V Filippova, S. K. J. Filatov, Journal of Molecular Structure **647**, 243 (2003).
[20] S. Nurten, and O. Halime, Solar Energy Materials & Solar Cells **126**, 56 (2014).
[21] S. Shadab, L. Khalid, H. Kevin, Journal of Applied Physics **103**, 094302 (2008).
[22] C. Yibing, K. Huizhen, D. Ju, W. Qufu, L. Jiulong, Z. Yong, S. Lei, H. Yuan, H. Fenglin, G. Weidong, F. Hao, Applied Energy **88**, 2106 (2011).
[23] H. E. Kissinger, Journal of Analytical Chemistry **29**(11), 1702 (1957).
[24] A.V. Arasu, A.S. Mujumdar, International Communications in Heat and Mass Transfer **39**(1), 8 (2012).
[25] C. J. Ho, J. Y. Gao, International Journal of Heat and Mass Transfer **62**, 2 (2013).